Electronic Supplementary Material (ESI) for Nanoscale Advances.


# Supplementary Information (SI)

# Metal-Organic Frameworks for Advanced Transducers based Gas Sensors: Review and Perspectives

Sanjit Manohar Majhi,[1] Ashraf Ali,[1] Prabhakar Rai,[2] Yaser E Greish,[3] Ahmed Alzamly,[3] Sandeep G. Surya,[4, 5] Naser Qamhieh,[1] and Saleh T. Mahmoud [1, *]

[1]Department of Physics, College of Science, United Arab Emirates University, Al-Ain 15551, United Arab Emirates

[2]Zoological Survey of India, Kolkata, 700053, India

[3]Department of Chemistry, College of Science, United Arab Emirates University, Al-Ain 15551, United Arab Emirates

[4]Sensors Lab, Advanced Membranes & Porous Materials Center (AMPMC), CEMSE, King Abdullah University of Science and Technology (KAUST), Thuwal 23955-6900, Saudi Arabia

[5]Sensor group, R&D Section, Dyson Tech. Limited, Malmesbury, United Kingdom

*Corresponding Author

E-mail address: saleh.thaker@uaeu.ac.ae (S. T. Mahmoud)

## 1. Fundamental Concepts and Working Principles of Advanced Transducers-based Gas Sensors

As discussed in the introduction of the main manuscript, based on the different transduction mechanisms, electrically-transduced gas sensors have been categorized into various types such as chemiresistive gas sensors, capacitive gas sensors, QCM gas sensors, and OFET gas sensors. In this section, we discuss the basic sensing principles of above electrically-transduced gas sensors.

### 1.1 Fundamental Principles of Chemiresistive based gas sensors

Typically, a chemiresistive based gas sensor is comprised of three components [1, 2] as follows (as shown in Fig. 1A);

1. The sensing layer (for recognizing the target gas).
2. Electrodes (for detecting the resistance changes).
3. A heater (for controlling the working temperature of the sensor)

Until now, MOXs based gas sensors are the most widely used sensing materials for chemiresistive gas sensors. The change of sensor resistance with respect to different gases (reducing or oxidizing) and sensing materials (*n-type* or *p-type* MOS) is the most widely accepted mechanism for a MOS-based chemiresistive sensor. When an *n*-MOS gas sensor is tested towards a reducing gas (e.g., $H_2S$, CO, $NH_3$, and $H_2$), the resistance of the sensor decreases, whereas it is the opposite for oxidizing gases (e.g., $SO_2$, $CO_2$, $NO_2$, and $O_3$). Similarly, it is the opposite sensing mechanism is proposed for a *p-type* MOS gas sensor [3-6], as shown in Fig. 1B.

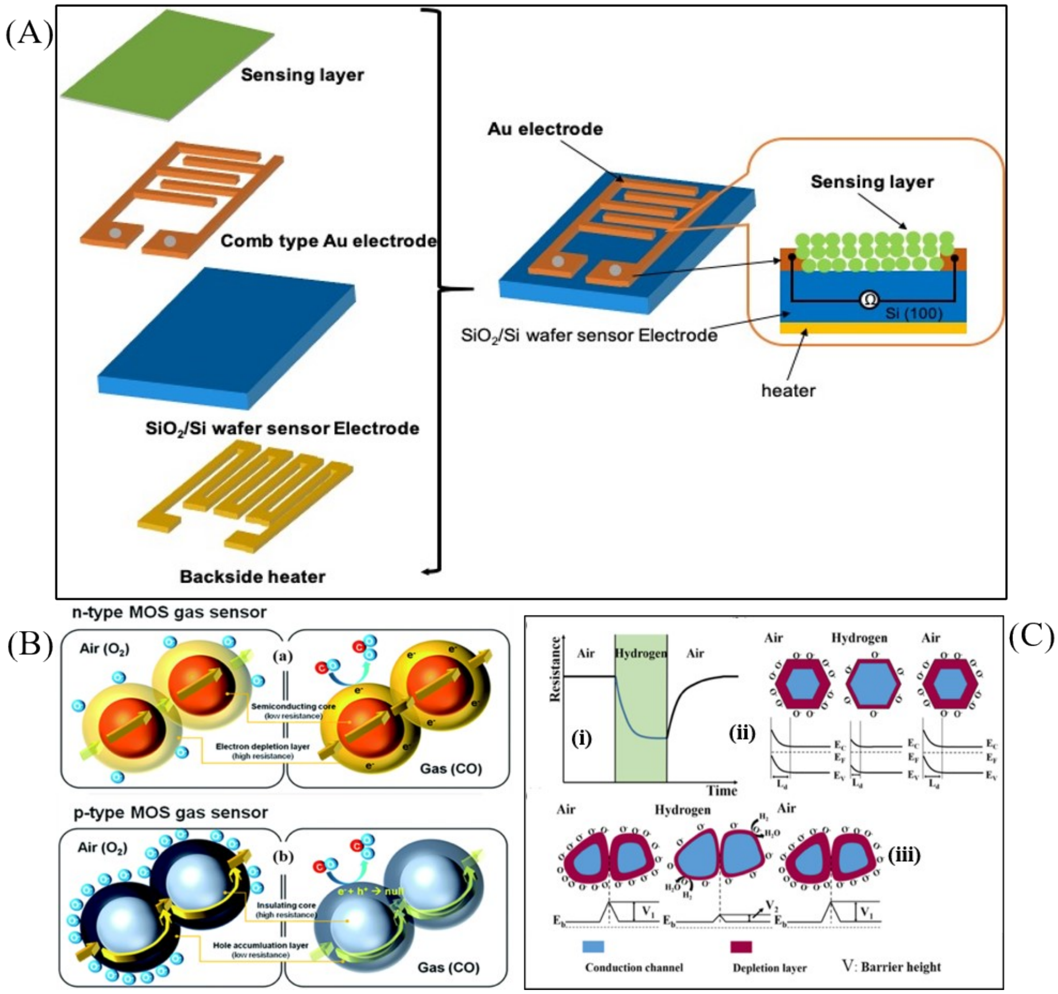


**Fig. 1** (A) Graphical representation of a typical chemiresistive type gas sensor comprises of electrodes, sensing layer, and a backside heater, (B) schematic representation of sensing mechanism of *n*-and *p-type* MOS gas sensors. Reprinted from the ref [7] with the permission of copyright 2021, Elsevier, and (C) Schematic model of change in the resistance of *n*-MOS throughout the detection of reducing gas ($H_2$) (a); Model of the surface charge layer (b); model of grain boundary barrier height in target gas and air environment (c). Reproduced from the ref [8] with the permission from Elsevier, copyright 2021.

The sensitivity of a gas sensor is significantly affected by the interaction between the sensing layer, adsorbed oxygen, and target gas [9]. There are two main adsorption processes, i.e., physisorption and chemisorption, involved at the sensor surface. In the physisorption process, the gas molecules are adsorbed at relatively lower operating temperatures; while in the chemisorption process, the charge transfer due to the bond formation between the adsorbed gas molecules and sensor surface atoms are involved [10]. Typically, when an n-type MOS sensor is air ambience, the $O_2$ molecules in the air are adsorbed on the sensing layer, thereby causing the conduction band (CB) electrons to be removed from the surface of MOX up to a certain depth. This leads to an increase in the negatively charged $O_2$ ions ($O_2^-$, $O^-$, $O^{2-}$) at the MOXs surface. The formation of these oxygen ionic species is highly dependent on operating temperatures [11].

For instance, at lower temperatures (25 to 150 °C), $O_2$ molecules form oxygen ion molecules, as defined in by the following equation:

$$O_{2(g)} + e^- \leftrightarrow O_2^-(ads) \tag{1}$$

At higher temperatures, the $O_2^-$ molecules are dissociated with either single or double oxygen ion atoms by taking an electron further from the CB of the sensor, according to the following equations:

$$\frac{1}{2}O_2 + e^- \leftrightarrow O^-(ads)\ (150 - 300\ ℃) \tag{2}$$

$$\frac{1}{2}O_2 + 2e^- \leftrightarrow O^{2-}\ (ads)(>300\ ℃) \tag{3}$$

Due to a negatively charged oxygen ion layer at the sensor's surface, an electron depletion layer or a space charge layer ($\Delta_{air}$) is created due to a low density of the electrons. This leads to an increase in the sensor's resistance in the presence of air and a subsequent decrease of the sensor's resistance in the presence of a reducing gas such as $H_2$ gas. The surface charge region with low electron concentration nearby the surface is called as the electron depletion layer (EDL). The depth of the EDL is referred to as Debye length ($L_d$) (Fig.1C (ii)), which is described as the distance between the surface of the metal oxide sensor to which the electrons are removed [12]. The presence of such depletion layer on the surface leads to band bending, as shown in Fig. 3C (ii).

The $L_d$ of a gas sensor is mostly reliant on the working temperature and concentration of charge carriers [13], which can be expressed as follows:

$$L_d = \sqrt{\frac{\varepsilon K_b T}{q^2 \times N_d}} \tag{4}$$

Here, $\boldsymbol{\varepsilon}$, $K_b$, T, q ($1.6 \times 10^{-19}$ C), and $N_d$ are the dielectric constant of the material, the Boltzmann constant, the operating temperature, electron charge, and concentration of charge carriers, respectively [14]. The conductivity of sensor materials is affected by the thickness of EDL.

On the other hand, beacuse the polycrystalline sensing materials are connected with numerous grain boundaries, the flow of electrons from one grain to another is prevented, resulting in the appearance of potential barrier (V) on the surface as shown in Fig. 3C (iii). As a result the sensor resistance increases. The height of potential barrier depends on the number of oxygen molecules adsorbed [15]. The dynamic interactions amongst the target gas (e.g., $H_2$) and the adsorbed oxygen species causes a change in carrier concentrations by releasing back the trapped electrons to the sensors, signal output, as a manifestation of the change of sensor resistance and decrease of potential barrier height [15, 16], according to the following equaions.

$$X + O_{ads}^{n-} \rightarrow X' + ne^- \tag{5}$$

where X, X', and n are the target gas, product gas, and the number of electrons released, respectively.

### 1.1.1 Basic Sensing Parameters

A gas sensor has basically 4 types of important parameters known as "4 S", which include sensitivity, selectivity, stability, and speed (response/recovery time). In addition, other parameters such as the limit of detection (LOD), repeatability, reproducibility. These parameters will be described here in more details [14].

(I) **Response:** The response of a gas sensor is defined as the ratio of change of electrically transduced sensor's signal in target gas and purging gas or carrier gas. For instance, the response of an n-type chemiresistive gas sensor toward a reducing gas in the air can be expressed by Eq. (6).

$$Response\ (R_S) = R_{air}/R_{gas} - 1 \tag{6}$$

Response also can be defined in the percentage (%), which can be expressed as follows [17];

$$R_S = \left[\frac{R_a - R_g}{R_a}\right] \times 100 \tag{7}$$

Where $R_{air}$, and $R_{gas}$ are the resistance change of in presence of air, and target gas conditions.

(II) **Sensitivity (S):** The term sensitivity is expressed as the change in resistance (ΔR) with the change in concentration of a target gas (ΔC). However, the response and sensitivity are not completely distinguished and, in many works, they seem identical in meaning. The sensitivity (S) can also be defined as the slope of the resistance or conductance change (dσ) of the gas sensors versus the change of concentration (dC) of gas molecules (equation 8) as follows;

$$S = d\sigma/dC \tag{8}$$

(III) **Response and Recovery Time:** The response time ($\tau_{res}$) can be defined as the time required for a gas sensor's signal to at least 90% change in the presence of analyte gas, whereas the recovery-time ($\tau_{rec}$) is defined as the 90% recovery of sensors' signal following the withdrawal of a target gas [15].

(IV) **Selectivity:** Selectivity is an essential parameter of chemiresistive sensors. The selectivity of a gas-sensing device is the ability to determine a specific gas among other interfering gases [16].

(IV) **Limit of Detection (LOD):** The LOD is defined as the ability to detect the lowest possible concentration of an analyte using a sensor at a particular operating temperature [18] at which the response is 3-fold higher than the standard deviation ($\sigma_{noise}$) of the baseline resistance ($R_a$) [19].

$$LOD = 3 \times rms_{noise}/S \qquad (9)$$

(V) **Long-term stability**: It is an important factor of a chemiresistive sensor too, and is defined as the capability of a gas sensor to provide repeatable results over a specified period [20].

### 1.2 Working principle of capacitive gas sensors

A capacitive gas sensor or simply called as chemicapacitor is a sensor device composed of two electrodes separated by an insulating layer or a dielectric layer such as air, MOFs, MOSs and mica, etc. that detects the changes in capacitance caused by dielectric interactions between gaseous analytes and insulating layers under an alternating current (AC) voltage. The basic sensing principle of capacitive-based sensors is the variation of capacitance of the sensing materials due to the change in dielectric permittivity ($\varepsilon_r$) upon adsorption of target gas/vapors molecules [21-23]. The capacitance (C, farads (F)) is generally expressed as follows [24]

$$C = \varepsilon_0 \varepsilon_r A/d \tag{10}$$

where C is the capacitance, $\varepsilon_0$ and $\varepsilon_r$ are the permittivity and relative permittivity, respectively, A is the electrode area, and d is the thickness of the dielectric layer [25, 26]. The response (Rs) of a capacitive gas sensor is calculated as follows;

$$Response\ (R_S) = \Delta C/C_{air} = \frac{\Delta I}{I_{air}} = \frac{C_{gas} - C_{air}}{C_{air}} = C_{air}/C_{air}\ -1 \tag{11}$$

Owing to their simple design, high compatibility with modern nanofabrication technology and ability to sense gas molecules at RT, capacitive-based gas sensors have been endowed as an excellent platform in sensing technology. The electrical transducer for capacitive-based gas sensors is generally found in two configurations: interdigitated electrode (IDE) and parallel-plate (PP), based on different sensing materials (as shown in Fig. 2a-b). An IDE structure has been used to sense the change in sensing film permittivity upon gas adsorption thereby leading to capacitive change. MOFs have been deployed as dielectric sensing layers for capacitive gas sensors, which play a significant role in the detection of various analytes [27].

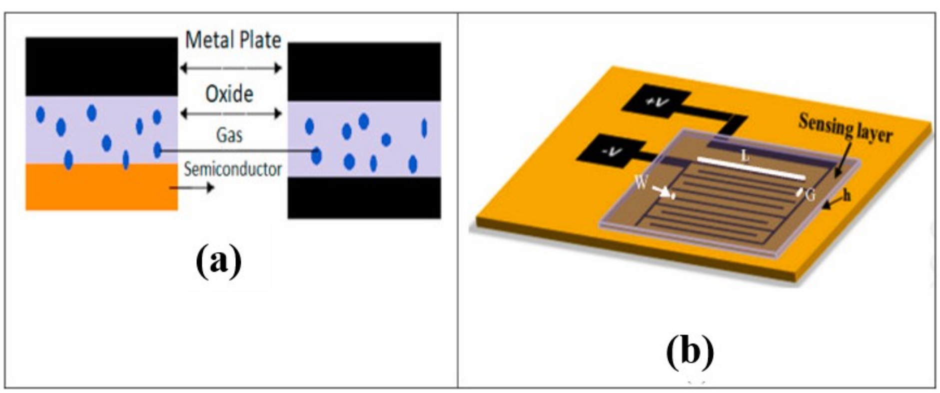


Fig. 2 (a-b) Schematic diagram of capacitive transducer with PP configuration and IDEs configuration, Reproduced from the ref [26] with the permission from Elsevier. Copyright 2021

### 1.3 Fundamental Principles of Quartz Crystal Microbalance gas sensors

Quartz crystal microbalance (QCM) based gas sensor is also classified in the coming under the mass sensitive sensors category. There are two types of mass sensitive sensors such as resonant microcantilever sensors and QCM sensors [28-30]. Owing to their conceptual simplicity, low power consumption, simple gravimetric-based sensing mechanism, and portability, QCM based gas sensors are gaining increased attention for the advancement of piezoelectric devices [31]. QCM is based on gravimetric principle and is utilized for the analysis of change of mass with shift of device resonance frequency [31]. A QCM sensor is comprised of a quartz disk connected metal electrodes on both sides (Fig. 3A). When a voltage is supplied to the QCM, it starts oscillating at a particular frequency. According to the principle, when the sensing material is coated on QCM substrate, the mass of sensing materials changes after adsorbing target gases. This change in mass (Δm) is recorded in the computer (as shown in Fig 3C) and transformed to the change of frequency (Δf). The relation between change of frequency (Δf) of the oscillating quartz crystal and the change in mass (Δm) on quartz crystal surface is described through the Sauerbrey equation X as follows [32];

$$\Delta F = -2.26 \times 10^{-6} f_0^2 \times \frac{\Delta m}{A} \qquad (12)$$

where ΔF is frequency change of sensing materials, $f_0$ is the fundamental resonance frequency (Hz), Δm is the loading of mass in g, and *A* is the surface area of QCM electrode ($cm^2$), respectively. When gas molecules are adsorbed on the surface of QCM transducer, a decrease of frequency is generated, whereas after the desorption of gas molecules, the sensor's frequency then returns back to the its baseline [33].

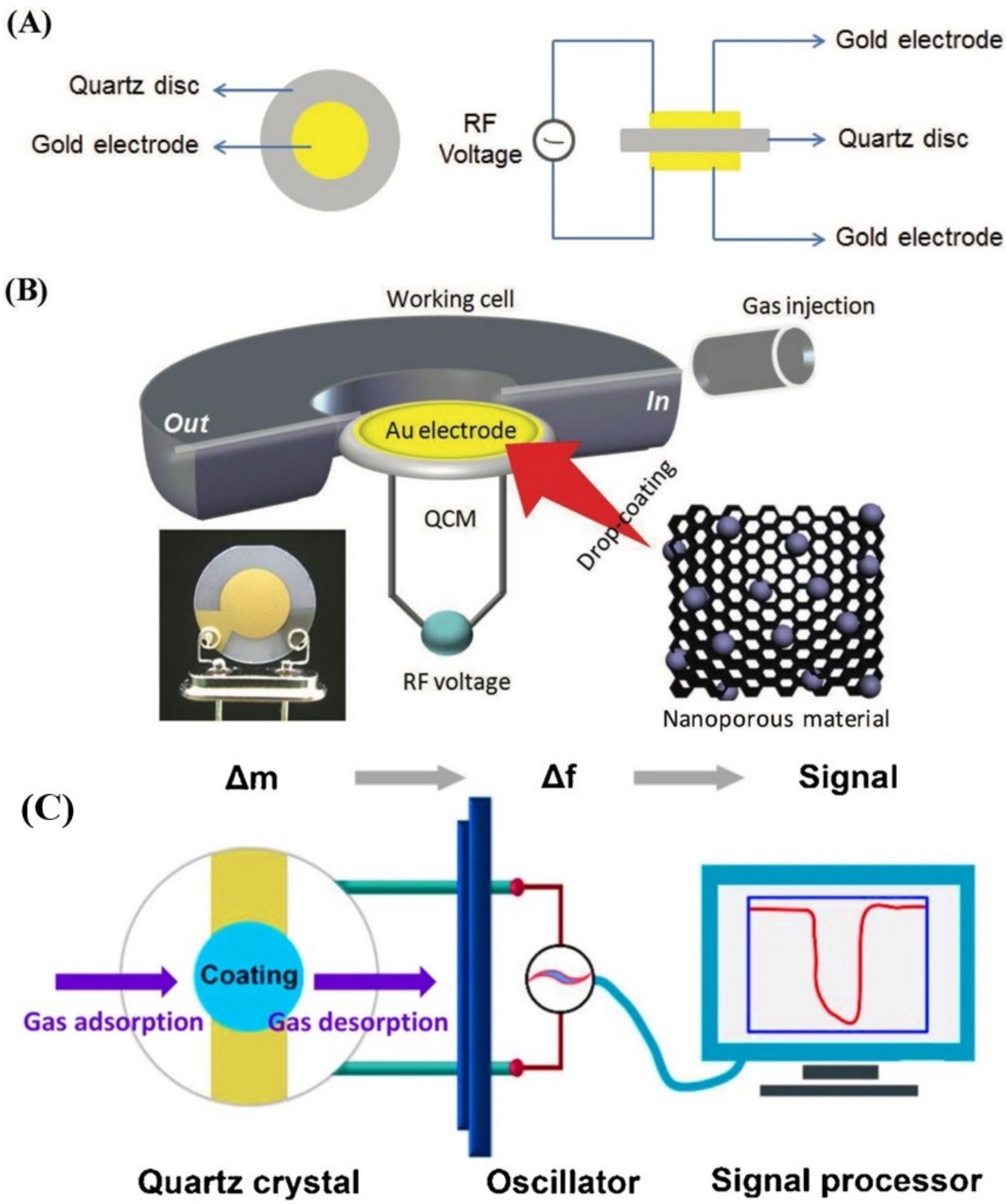


Fig. 3 Schematic diagram of (A-B) QCM electrode. Showing the interaction between sensing layer and the target molecules. Reproduced from the ref [32], Copyright @2021, Wiley-sons, and

(C) schematic diagram of working principle and experimental setup of QCM. Reprinted from the Ref [34], copyright@202, Elsevier.

### 1.4 Fundamental concepts of Organic Field-Effect Transistor gas sensors

OFET based gas sensors can exhibit fingerprint response for the detection of a variety of gas molecules at low concentrations. They consist of three layers: the first layer, a dielectric layer, and source-drain and gate electrodes. They are mainly designed using a bottom-gate approach (as shown in Fig. 4A) due to its direct interaction with OSC/ analyte. However, based on their device structures OFET sensors can be divided into four categories such as bottom gate/bottom contact (BGBC), bottom gate/top contact (BGTC), top gate and top contact (TGTC), and top gate/bottom contact (TGBC) according to their deposition order of OSC, dielectric, and metals [35, 36]as shown in Fig. 4 (B(i-iv)).

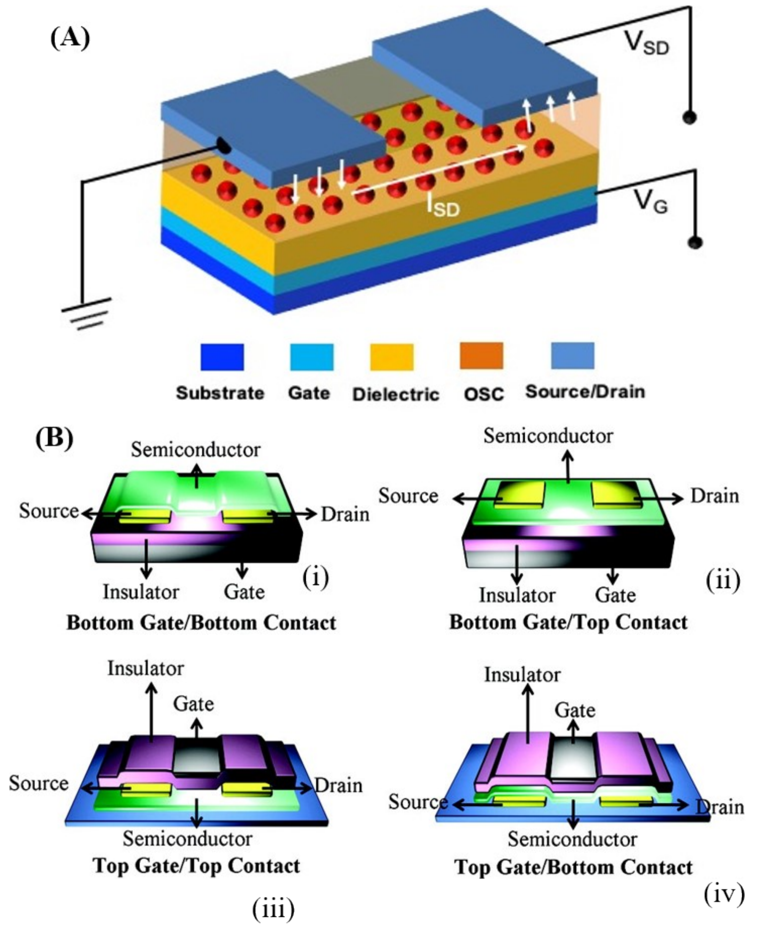


Fig. 4 (A) Schematic diagram of a typical three terminal based OFET based device structure, where $V_{SD}$ is the drain voltage, $V_G$ is the gate bias voltage and $I_{SD}$ is the current flow, and (B) Schematic diagrams of four kinds of OFET device structures such as (i) BGBC; (b) BGTC; (c) TGTC; and (d) TGBC. Fig. 28(B) Reprinted from the ref [37]. Copyright 2021@ the creative commons Attribution License, MDPI.

Among these OFET sensors, BGBC and BGTC are used mostly, while TGTC and TGBC are popularly used in MOSFET based sensor. The transduction mechanism of OFET devices in the presence of target gases is attributed to the change in the current at the dielectric /organic semiconductor layer interface ($I_{SD}$). The analyte binding with the organic semiconductor layer would convert to an easily recorded electrical signal using the OFET transducer-based platform. The charge carrier transportation in conducting channel can either be increased or decreased depending on the gas–OSCs interaction, especially when it is taken care of by the π-conjugated system of OSC. The modulation of gate voltage ($V_{SD}$) controls the flow of current between the source and drain electrodes. At given $V_{SD}$ and VG, the response of OFET gas sensor (n-type) towards reducing gases is expressed as follows;

$$Response = \frac{\Delta I_{SD}}{I_{SD(air)}} = \frac{I_{SD\,(gas)} - I_{SD\,(air)}}{I_{SD(air)}} = \frac{I_{SD\,(gas)}}{I_{SD\,(air)}} - 1 \tag{13}$$

In addition, the current flow can be affected by different factors such as morphology and/or energy levels of OSC and test gas molecules [38]. One of the main advantages of OFETs is that multiple parameters ($\mu_{FET}$, $I_{on}/I_{off}$, and $V_T$) can be used to evaluate their sensing performance.

References:


1 D.R. Miller, S.A. Akbar, and P.A. Morris, *Sens. Actuators*, B 2014, **204**, 250-272.

2 P. Gao, R. Liu, H. Huang, X. Jia, and H. Pan, *RSC Adv.* 2016, **6(97)**, 94699-94705.

3 K. Vellingiri, A. Deep, and K.-H. Kim, *ACS Appl. Mater. Interfaces* 2016, **8(44)**, 29835-29857.

4 X. Fang, B. Zong, and S. Mao, *Nano-Micro Lett.* 2018, **10(4),** 1-19.

5 F. Xu, and H.-P. Ho, *Micromachines* 2017, **8(11)**, 333.

6 A.A. Baharuddin, B.C. Ang, A. Haseeb, Y.C. Wong, and Y.H. Wong, Mater. Sci. Semicond. Process. 2019, **103**, 104616.

7 P. Rai, S.M. Majhi, Y.-T. Yu, and J.-H. Lee, *RSC Adv.* 2015, **5(93)**, 76229-76248.

8 S.M. Majhi, A. Mirzaei, H.W. Kim, S.S. Kim, and T.W. Kim, *Nano Energy* 2020, 79, 105369.

9 M.E. Franke, T.J. Koplin, and U. Simon, *Small* 2006, **2(1),** 36-50.

10 J.M. Walker, S.A. Akbar, and P.A. Morris, *Sens. Actuators, B* 2019, **286**, 624-640.

11 A. Dey, *Mater. Sci. Eng., B* 2018, **229**, 206-217.

12 N. Yamazoe, *Sens. Actuators, B* 2005, **108(1-2)**, 2-14.

13 Y.J. Kwon, H.G. Na, S.Y. Kang, M.S. Choi, J.H. Bang, T.W. Kim, A. Mirzaei, and H.W. Kim, *Sens. Actuators, B* 2017, **239,** 180-192.

14 K.J. Choi, and H.W. Jang, *Sensors* 2010, **10(4**) 4083-4099.

15 A. Mirzaei, J.-H. Lee, S.M. Majhi, M. Weber, M. Bechelany, H.W. Kim, and S.S. Kim, *J. Appl. Phys.* 2019, **126(24),** 241102.

16 A. Gurlo, N. Bârsan, U. Weimar, Gas sensors based on semiconducting metal oxides, CRC press, 2005, pp. 705-760.

17 D. Kukkar, K. Vellingiri, R. Kaur, S.K. Bhardwaj, A. Deep, and K.-H. Kim, *Nano Res.* 2019, **12(2),** 225-246.

18 R. Kumar, O. Al-Dossary, G. Kumar, and A. Umar, *Nano-Micro Lett.* 2015, **7(2)**, 97-120.

19 W.-T. Koo, J.-S. Jang, and I.-D. Kim, *Chem* 2019, **5(8)**, 1938-1963.

[20] F. Gu, C. Li, D. Han, and Z. Wang, *ACS Appl. Mater. Interfaces* 10(1) (2018) 933-942.

21 S. Sachdeva, M.R. Venkatesh, B.E. Mansouri, J. Wei, A. Bossche, F. Kapteijn, G.Q. Zhang, J. Gascon, and L.C. de Smet, E.J. Sudhölter, *Small* 2017, **13(29)**, 1604150.

22 C. Sapsanis, H. Omran, V. Chernikova, O. Shekhah, Y. Belmabkhout, U. Buttner, M. Eddaoudi, and K.N. Salama, Sensors 2015, **15(8),** 18153-18166.

23 T. Ishihara, and S. Matsubara, *J. Electroceram*. 1998, **2(4),** 215-228.

24 K. Vikrant, V. Kumar, Y.S. Ok, K.-H. Kim, and A. Deep, *TrAC, Trends Anal. Chem.* 2018, 105, 263-281.

25 K. Dutta, N. Banerjee, H. Mishra, and P. Bhattacharyya, *IEEE Trans. Electron Devices* 2016, **63(3)**, 1266-1273.

26 A. Nasri, M. Petrissans, V. Fierro, and A. Celzard, *Mater. Sci. Semicond. Process*. 2021, **128**, 105744.

27 S. Zeinali, S. Homayoonnia, G. Homayoonnia, *Sens. Actuators, B* 2019, **278**, 153-164.

28 S. Ha, M. Lee, H.O. Seo, S.G. Song, K. S. Kim, C.H. Park, I.H. Kim, Y.D. Kim, and C. Song, *ACS Sens.* 2017, **2(8)** ,1146-1151.

29 J. Lin, N. Gao, J. Liu, Z. Hu, H. Fang, X. Tan, H. Li, H. Jiang, H. Liu, T. Shi, *J. Mater. Chem. A* 2019, **7(15),** 9068-9077.

30 S. Cai, W. Li, P. Xu, X. Xia, H. Yu, S. Zhang, X. Li, *Analyst* 2019, **144(12),** 3729-3735.

31 R. Roto, A. Rianjanu, A. Rahmawati, I.A. Fatyadi, N. Yulianto, N. Majid, I. Syamsu, H.S. Wasisto, and K. Triyana, *ACS Applied Nano Materials* 2020, **3(6),** 5687-5697.

32 N.L. Torad, S. Zhang, W.A. Amer, M.M. Ayad, M. Kim, J. Kim, B. Ding, X. Zhang, T. Kimura, Y. Yamauchi, *Adv. Mater. Interfaces* 2019, **6(20),** 1900849.

33 L. Wang, Sens. Actuators, A 2020, **307**, 111984.

34 Z. Ma, T. Yuan, Y. Fan, L. Wang, Z. Duan, W. Du, D. Zhang, and J. Xu, *Sens. Actuators, B* 2020, **311**, 127365.

35 C. Zhang, P. Chen, and W. Hu, Chem. Soc. Rev. 2015, **44(8),** 2087-2107.

36 S.G. Surya, H.N. Raval, R. Ahmad, P. Sonar, K.N. Salama, and V.R. Rao, *TrAC, Trends Anal. Chem.* 2019, **111**, 27-36.

37 A. Lv, Y. Pan, and L. Chi, *Sensors* 2017, **17(1)**, 213.

38 S. Yuvaraja, A. Nawaz, Q. Liu, D. Dubal, S.G. Surya, K.N. Salama, and P. Sonar, *Chem. Soc. Rev.* 2020, **49(11)**, 3423-3460.